Spatial distribution of the doped electrons in cubic $Sr_{1-x}La_xMnO_3$ ($x \leqslant 0.04$) oxides probed by ^{87}Sr NMR

A. Germov,[1] A. Trokiner,[2] Z. Volkova,[1] K. Mikhalev,[1] A. Gerashenko,[1,2] S. Verkhovskii,[1,2] A. Korolev,[1] I. Leonidov,[3] E. Konstantinova,[3] and V. Kozhevnikov[3]

[1]*Mikheev Institute of Metal Physics, Ural Branch of Russian Academy of Sciences, 620990 Ekaterinburg, Russia*

[2]*ESPCI Paris, PSL Research University, CNRS, Sorbonne Universités, UPMC, LPEM, 10 rue Vauquelin, Paris, France*

[3]*Institute of Solid State Chemistry, Ural Branch of Russian Academy of Sciences, 620990 Ekaterinburg, Russia*

(Received 5 July 2017; published 7 September 2017)

The spin density of doped electrons was investigated by ^{87}Sr NMR in the paramagnetic (PM) and antiferromagnetic (AF) G-type phases of electron-doped $Sr_{1-x}La_xMnO_3$ ($x = 0.00, 0.02, 0.04$; $T_N = 236$–200 K) ceramics with the cubic structure. It is shown that the ^{87}Sr NMR shift is proportional to the local density of the itinerant doped electrons surrounding the Sr sites; these electrons have mainly the e_g character. In the PM phase, all the doped electrons are itinerant; however, they are inhomogeneously distributed in the La-containing oxides, creating electron-doped regions (EDRs) with a number of e_g electrons per Mn larger than in the rest of the oxide. At room temperature, the network of the overlapping EDRs does not cover all Sr sites. Nevertheless, the number of the Sr sites inside an EDR exceeds the site percolation threshold even for $x = 0.02$, so that the e_g electrons can move on large distances. In the AF phase, below 80 K the EDRs cover the entire crystal. In this T range the doped electrons separate into two species: some of them slow down their motion and form below 50 K static FM domains, which are considered as bound magnetic polarons (MPs) of small size with the effective moment $p_{eff} = 23(10)\ \mu_B$ and a MP formation energy ~40 meV. The second species concerns the electrons which remain itinerant at low temperature participating in the fast hopping in the AF G-type ordered lattice of the Mn^{4+} ions. Nevertheless, their motion is slower than what is expected in an AF metal phase without cation disorder; this is probably due to the imperfect shielding of the (La^{3+}/Sr^{2+}) charge disorder.

DOI: 10.1103/PhysRevB.96.104409

I. INTRODUCTION

The manganites display a great variety of electronic properties when doped by charge carriers [1]. One of the main issues in the studies of these strongly correlated materials is the ground state emerging from the competition of the antiferromagnetic (AF) superexchange (SE) interaction between localized spins and the ferromagnetic (FM) double-exchange (DE) interaction of the localized spins with the itinerant doped carriers [2,3]. On the insulating side of the FM metal to AF insulator transition (MIT) the magnetic ground state of the doped $Sr_{1-x}La_xMnO_3$ and $Ca_{1-y}La_yMnO_3$ oxides is considered as heterogeneous with FM nanosize domains frozen in the AF lattice, the doping being whether with holes ($x, y > 0.7$) [4–6] or with electrons ($x < 0.1$ [7,8], $y < 0.1$ [9–12]). In the hole-doped oxides, a magnetic field induces the percolation of these FM domains [13,14] yielding a MIT with the colossal magnetoresistance (CMR) effect [15] which is nowadays widely used in spintronics.

The parent compounds, $CaMnO_3$ (orthorhombic, $Pnma$; $T_N \approx 120$ K [16,17]) and $SrMnO_3$ (cubic, $Pm3m$; $T_N \approx 240$ K [18,19]) have a simple AF G-type order of the core $S(t_{2g})$ spins of the Mn^{4+} ($^3t_{2g}{}^0e_g$; $S = 3/2$) ions. The heterovalent substitution of Ca^{2+} or Sr^{2+} with La^{3+} (Ce^{4+}) donates one (two) extra electron(s) to the e_g conduction band and shifts these semiconducting oxides toward the MIT. In the paramagnetic (PM) phase, the resistivity, ρ, is lowered by several orders of magnitude due to a rather small number of doped electrons ($x \geqslant 0.01$ [8], $y \geqslant 0.02$ [20]) yielding a crossover to a metallic-like behavior ($d\rho/dT > 0$) above room temperature.

In the AF G-type phase, at low temperature where the magnetic scattering of the conduction electrons by the t_{2g} spins vanishes, the residual resistivity $\sim 10^{-2}\ \Omega$ cm [8] is significantly larger than the value expected for the AF metal ground state [21,22]. The low mobility of the dilute carriers was tentatively assigned to their enhanced coupling with the Jahn-Teller phonons [8,20]. However, almost no polaronic renormalization of the e_g electron mass follows from a microscopic model of $Sr_{1-x}La_xMnO_3$ and $Sr_{1-x/2}Ce_{x/2}MnO_3$ oxides [22]. According to this model at low doping level, the e_g electrons move with a reduced velocity due to the narrowing of the conduction band in the AF G-type phase. These controversial interpretations require more details about the motion of the itinerant doped electrons, about the locally varying competition of the DE and SE interactions, and about the corresponding AF/FM configuration of the neighboring t_{2g} spins.

In the AF phase of the electron-doped cubic $SrMnO_3$ the DE/SE competition is manifested by a static FM component, M_{FM}, emerging in the bulk magnetization at low temperature [8,23]. Whether M_{FM} should be assigned to the canted AF G-type structure or to the nanosize FM entities is a dilemma which can be resolved with neutron scattering and/or NMR experiments. The ^{55}Mn NMR study of lightly electron-doped $Sr_{1-x}La_xMnO_3$ ($x = 0.02$) [24] compounds has shown two well resolved NMR signals corresponding to the AF and FM correlated Mn spins, evidencing the separation of the doped electrons into two species and the heterogeneity of the magnetic ground state.

In this paper we present a ^{87}Sr NMR study of lightly electron-doped cubic $Sr_{1-x}La_xMnO_3$ ($0.0 \leqslant x \leqslant 0.04$) polycrystalline samples. The magnetic state of these oxides is characterized by the bulk magnetization with a focus on the

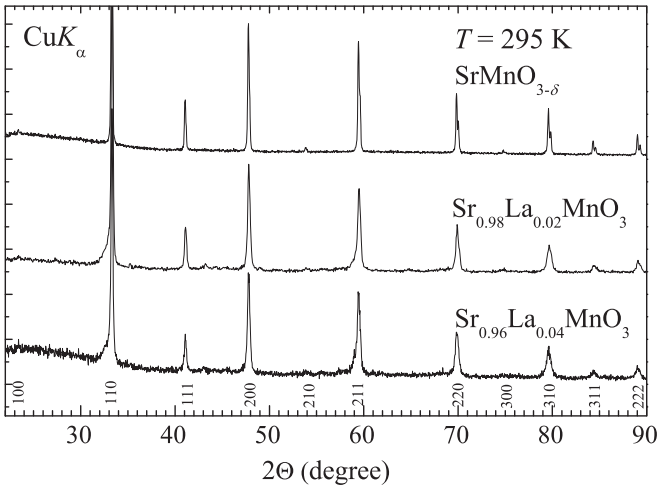

FIG. 1. X-ray diffraction powder pattern of the $Sr_{1-x}La_xMnO_{3-\delta}$ ($x = 0.00, 0.02, 0.04$) samples measured with the CuK_α radiation at room temperature.

static M_{FM} component emerging in the AF phase (Sec. III A). In $Sr_{1-x}La_xMnO_3$ the resonance frequency of ^{87}Sr (nuclear spin $^{87}I = 9/2$ and the quadrupole moment $^{87}Q = 0.15 \times 10^{-24}$ cm^2) is determined by both the magnetic hyperfine and the electric quadrupolar interactions, so that with the ^{87}Sr NMR tool we can probe the spatial distribution of the spin and charge densities with a resolution of about the cubic unit cell size. The negligible quadrupole broadening of the ^{87}Sr NMR spectrum complements the room temperature x-ray diffraction data, evidencing that the average crystal symmetry of the studied samples is cubic in both the PM and AF phases (Sec. III B 1). The magnetic hyperfine interaction of ^{87}I with the itinerant doped electrons coupled by DE with eight Mn^{4+} neighbors and its impact on the magnetic broadening of the ^{87}Sr NMR in the La-containing oxides is clarified in Secs. III B 3 and III B 4. As a result, the variation with T and x of a spatially distributed density of the itinerant e_g electrons is disclosed in the La-doped oxides. At low temperature, the separation of the e_g electrons into two species with a distinct thermal behavior is quantitatively characterized by the ^{87}Sr spin-lattice relaxation rate, $^{87}T_1^{-1}$, in Sec. III C and by the ^{87}Sr spin-echo decay rate, $^{87}T_2^{-1}$, in Sec. III D.

II. EXPERIMENTAL DETAILS

The $Sr_{1-x}La_xMnO_{3-\delta}$ samples ($x = 0.02, 0.04$) were synthesized with the citrate-gel method [25]. Thoroughly milled chemically pure (99.9%) initial reagents $SrCO_3$, La_2O_3, and Mn_2O_3 were weighted in the right quantities and put into a quartz ampoule with nitrogen acid until complete dissolution. After that, citrine acid was added until getting a homogeneous gel which was heated to ignition. The black powder obtained was pressed into tablets of 2 mm thickness and 12 mm diameter. The tablets were first annealed at 900 °C in air for 2 hours and then the annealing temperature was increased up to 1300 °C. After 10 hours the samples were cooled down to room temperature, with a cooling rate ∼1 °C per minute. According to x-ray diffraction (XRD) data, the samples adopt the hexagonal $4H$-$SrMnO_3$ structure with a minor volume fraction of the $6H$-$SrMnO_3$ polymorph.

In order to obtain the $x = 0.02$ and 0.04 samples with the cubic structure, we used the two-stage method which was developed for similar metastable compounds [19]. At the first stage the samples were heated in a flow of gas mixture 10% H_2 / 90% Ar up to 1000 °C until the oxygen content had decreased to $(3–\delta) \approx 2.55$. The reduction reaction was permanently monitored with a thermal analyzer Setaram TG-92. The XRD analysis showed that after reduction, a single-phase oxygen-deficient sample with $Sr_2Mn_2O_5$ structure was formed. In order to achieve 3 oxygen atoms per formula unit the samples were finally annealed at 400 °C in air.

The $SrMnO_{3-\delta}$ ($\delta < 0.005$) polycrystalline sample with cubic structure was synthesized with the procedure described in Ref. [23]. At the last stage of synthesis the sample was annealed (24 hours $T = 500$ °C) in oxygen flow ($P_{O_2} \sim 1$ bar) containing ∼70% of ^{17}O isotope, for ^{17}O NMR measurements.

The XRD patterns, measured with the CuK_α radiation, at 295 K confirm that the three synthesized samples are single phase (Fig. 1) since only the Bragg reflections corresponding to the cubic structure are observed. The RT cubic unit cell parameter, a, listed in Table I, shows that the size of the cubic cell increases with La doping.

Magnetization measurements were carried out in the temperature range $T = 4–330$ K and in external magnetic fields $H \leqslant 9$ T with a magnetometer PPMS 9 (Quantum Design).

The ^{87}Sr NMR spectra were measured between 20 K and 370 K, with a Bruker NMR spectrometer AVANCE 500 WB in an external magnetic field $H_0 = 11.747$ T. The spin echo signals were excited by the pulse sequence $\pi/2$-τ-$\pi/2$ with $\pi/2$ pulse length equal to 2 μs. The spectra extending to more than 200 kHz were obtained by summing the Fourier-transformed half-echo signals acquired at equidistant (∼100 kHz) operating frequencies. The ^{87}Sr NMR shift components were determined with respect to the ^{87}Sr Larmor frequency, $\nu_0 = 21.6747$ MHz.

TABLE I. Cubic unit cell parameter at room temperature, a, Néel temperature, T_N, magnetic width, $\Delta\nu_M$, and quadrupolar width, $\Delta\nu_Q$, at $H = 11.7$ T, $T = 300$ K of the ^{87}Sr spectra.

	$SrMnO_{3-\delta}$ ($\delta < 0.005$)	$Sr_{0.98}La_{0.02}MnO_3$	$Sr_{0.96}La_{0.04}MnO_3$
a ($T = 295$ K) (Å)	3.8062(4)	3.8068(6)	3.8095(8)
T_N (K)	236(4)	230(10)	200(20)
$(\Delta\nu)_M$ (kHz)	5	18	35
$(\Delta\nu)_Q$ (kHz)	10(1)	37(4)	43(4)
$(\delta\nu)_Q = (\Delta\nu)_Q^2/\nu_0$ (kHz)	0.01	0.2	0.24

The simulation of the spectra of the polycrystalline samples allows us to determine the hyperfine interaction parameters, i.e., the isotropic shift, $^{87}K_{\rm iso} = (\nu - \nu_0)/\nu_0$, the value of the quadrupole frequency $\nu_Q = [3e^2Q/2I(2I-1)h]V_{zz}$ which characterizes the interaction of the quadrupole moment ^{87}Q with V_{zz}, the main component of the electric field gradient at the Sr sites. The Gaussian widths $\Delta K = \Delta\nu_M/\nu_0$ and $\Delta\nu_Q$ of the distribution of $^{87}K_{\rm iso}$ and ν_Q, respectively, were also evaluated at the Sr sites.

The ^{87}Sr spin-lattice relaxation time, T_1, was measured with the pulse sequence, $\pi/2$-τ-$\pi/2$-$E(2\tau,t)$ by varying t, the repetition time. The recovery of the nuclear magnetization towards equilibrium conditions was always exponential.

The spin-spin relaxation time, T_2, has been measured using the pulse sequence $\pi/2$-τ-π. The T_2 value was determined as the time interval 2τ during which the echo signal $E(2\tau)$ drops to $1/e$ of its initial value. Both T_1 and T_2 were measured on the peak of the central line (transition $m_{\rm I} = -1/2 \leftrightarrow +1/2$).

III. RESULTS AND DISCUSSION

A. Magnetic susceptibility

The temperature dependence of the magnetic susceptibility $\chi = M/H$ obtained by field-cooling at $H = 9$ T is shown in Fig. 2(a). The transition temperature to the AF G-type ordered phase, $T_{\rm N}$, is determined from the position of the maximum of $d\chi/dT$ [inset in Fig. 2(a)]. With increasing x, $T_{\rm N}$ diminishes (Table I) in agreement with data obtained in single crystals of the same composition [8]. Moreover, according to Ref. [8], the presence of a local maximum [$T_{\rm N2} \approx 100(20)$ K] in $d\chi/dT$ for the $x = 0.04$ sample may indicate the formation of a AF C-type structure in a part of the sample.

The field dependence of the magnetization, M, is seen in the $M(H)$ reversal isotherms [Fig. 2(b)] obtained up to 9 T, by cooling from $T = 330$ K. In the AF phase each $M(H)$ isotherm can be represented as the sum of two contributions:

$$M(H) = M_{\rm AF} + M_{\rm FM}, \qquad (1)$$

where $M_{\rm AF} \propto H$ is the magnetization of the canted-in-magnetic-field AF G-type structure. The FM component $M_{\rm FM}(H) = M(H) - M_{\rm AF}(H)$ varies nonlinearly with H towards the maximum value $M_{\rm FM,sat}$ at $H > 3$ T.

The origin of $M_{\rm FM}$ was clarified in a ^{55}Mn NMR study [24] of the very same $x = 0.02$ sample. Indeed, the ^{55}Mn NMR spectra show two well resolved lines which were assigned to Mn atoms in the AF lattice and in FM domains, evidencing the heterogeneity of the magnetic ground state. In this study, we present more detailed properties of $M_{\rm FM}$ at low temperature.

(a) The thermal behavior of $M_{\rm FM,sat}$ and $N_{\rm FM}$, the fraction of the Mn atoms located inside the FM domains, is represented in the inset of Fig. 2(b), for the $x = 0.02$ sample. The $N_{\rm FM}$ value was estimated from ^{55}Mn NMR by measuring the intensity of the FM line, $^{55}Int_{\rm FM\text{-}line} \propto N_{\rm FM}/T$, which obeys the Curie law. As T increases, the drop of $M_{\rm FM,sat}$ and $N_{\rm FM}$ are about the same ($\approx$3 times) indicating that the decrease of $M_{\rm FM,sat}$ is determined by $N_{\rm FM}$. Above 80 K about 2/3 of the Mn atoms are no longer FM coupled and the corresponding FM-ordered entities vanish.

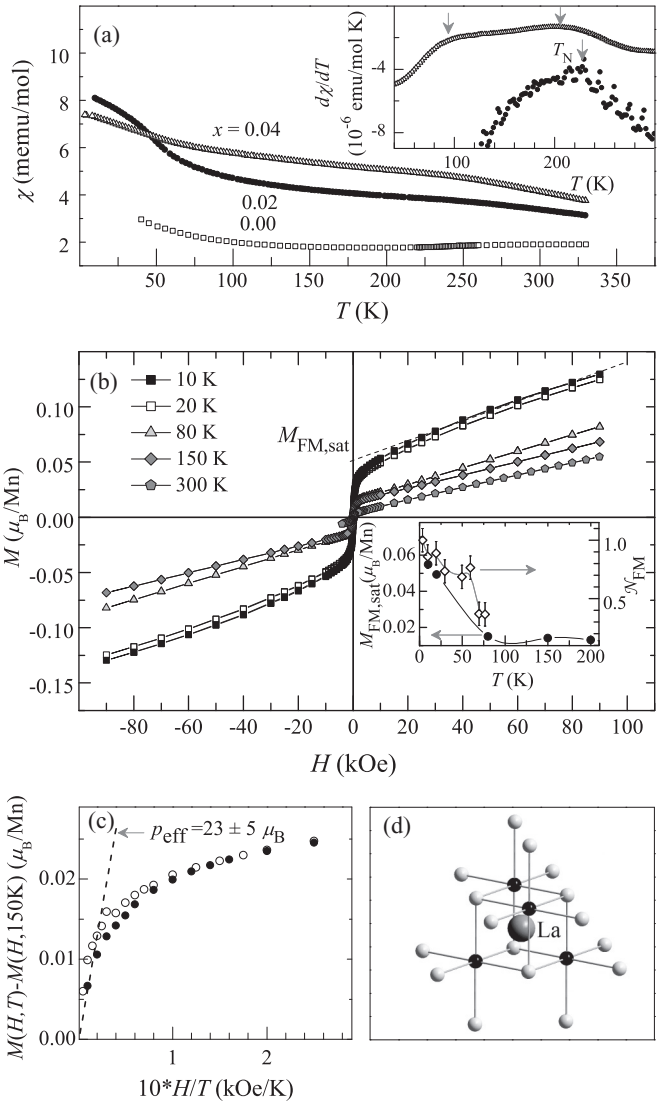

FIG. 2. (a) Magnetic susceptibility $\chi(T) = M/H$ measured by cooling $Sr_{1-x}La_xMnO_3$ [$x = 0.00$ (□), 0.02 (•), 0.04 (△)] in a magnetic field $H = 9$ T. Inset: derivative $\Delta\chi/\Delta T$ vs T for $x = 0.02$ and 0.04 samples; the transition temperature, $T_{\rm N}$, is indicated by arrows. (b) Magnetization reversal isotherms $M(H)$ of $Sr_{0.98}La_{0.02}MnO_3$. Inset: fraction $N_{\rm FM}$ (◊) of the Mn atoms located inside the static FM entities, and $M_{\rm FM,sat}(T)$ (•) vs temperature. (c) Magnetization $[M(H,T) - M(H,T = 150\ {\rm K})]$ vs H/T in $Sr_{0.98}La_{0.02}MnO_3$ at $T = 10$ K (•) and $T = 20$ K (○). The dashed line is the initial slope of the Langevin function: $M = (p_{\rm eff}^2/3k_{\rm B})H/T$ with the effective magnetic moment $p_{\rm eff} = 23(10)\ \mu_{\rm B}$. (d) Schematic fragment of the cubic structure: the gray balls indicate the Mn atoms with spin down in the AF G-type lattice whereas the spin up of the four Mn represented by black balls is flipped to form the magnetic polaron, $m_{\rm MP} = 25\ \mu_{\rm B}$, centered at the La cation.

(b) The magnetization of these thermally unstable FM entities, defined as the difference $[M(H,T) - M(H,T = 150\ {\rm K})]$, is presented vs H/T [Fig. 2(c)] in a Langevin plot for $T = 10$ K and 20 K, in order to underline the particular thermal behavior that is observed in single-domain FM nanoparticles with negligible crystallographic and shape anisotropies. The dashed line shows the initial slope (in weak magnetic fields)

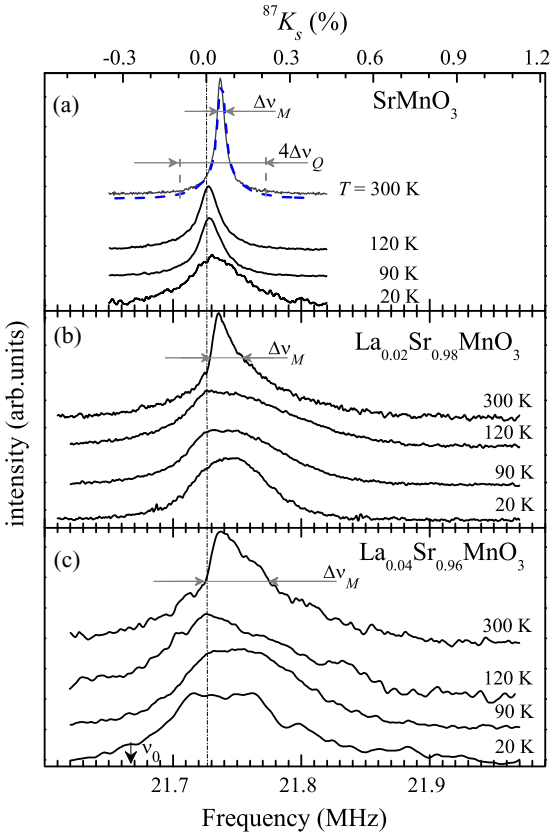

FIG. 3. ^{87}Sr NMR spectra obtained at 11.7 T in the polycrystalline $x = 0.00$ (a), 0.02 (b), 0.04 (c) samples at $T = 300$, 120, 90, and 20 K; $\Delta\nu_M$ is the width at half height of the central transition $m_I = -1/2 \leftrightarrow +1/2$, and $\Delta\nu_Q$ is the width at half height of the satellite transition $m_I = 1/2 \leftrightarrow 3/2$. The blue dashed curve shows the ^{87}Sr NMR spectrum including all transitions ($x = 0.00$; $T = 300$ K), calculated with $\nu_Q = 0$ and with the $\Delta\nu_M$ and $\Delta\nu_Q$ values listed in Table I.

of the Langevin function, $M = (p_{\text{eff}}^2/3k_B)H/T$, yielding the effective magnetic moment value $p_{\text{eff}} = 23(10)\ \mu_B$ per FM entity. A possible configuration of these FM clusters in $Sr_{1-x}La_xMnO_3$ is shown in a fragment of the AF G-type cubic structure centered on a La atom with 20 Mn atoms [Fig. 2(d)]. Due to the DE interaction, a doped electron trapped inside this fragment flips the spins of the four Mn^{4+} ions shown by black balls, so that all 20 Mn spins are FM polarized, creating a bound magnetic polaron (MP) with a magnetic moment $m_{\text{MP}} = 25\ \mu_B$ [26], close to the value previously deduced. Besides, the negligible hysteresis ($H_{\text{coerc}} \leqslant 0.001$ T), observed in the $M_{\text{FM}}(H)$ reversal isotherms [Fig. 2(b)], is in agreement with the rather high symmetry of this MP.

B. ^{87}Sr NMR spectra

1. *Quadrupole interaction and cubic symmetry*

Figure 3 shows examples of ^{87}Sr NMR spectra obtained in the three polycrystalline samples. The spectra consist of a central line transition ($m_I = -1/2 \leftrightarrow +1/2$) with a relative intensity of 15%, centered on a wide pedestal of 8 unresolved satellite line transitions ($2I - 1 = 8$). For quadrupole nuclei, such unresolved NMR spectrum is usually detected in a powder of imperfect cubic crystals [27]. As shown by our XRD data, the average symmetry of the 3 samples is cubic at 300 K. This yields $\langle V_{zz}\rangle \propto \langle \nu_Q\rangle = 0$ for the electric field gradient and the quadrupole frequency. Nevertheless, the locally distorted cubic symmetry at the Sr sites produces electric field gradient (EFG) local perturbations, $|V_{zz} - \langle V_{zz}\rangle|$, which lead to the existence of satellite lines. The width of these lines is characterized by $\Delta\nu_Q$ whereas the central line is broadened by $\delta\nu_Q = (\Delta\nu_Q)^2/\nu_0$, which is far smaller than $\Delta\nu_Q$ so that the width of the central line, $\Delta\nu_M$, is only due to the magnetic interaction.

For instance, the dotted blue curve in Fig. 3(a) results from the simulation with $\langle\nu_Q\rangle = 0$ of the room-temperature NMR spectrum of $SrMnO_{3-\delta}$. The optimized broadening $\Delta\nu$ and $\Delta\nu_Q$, given in Table I, show that a small deviation from the stoichiometric composition ($\delta < 0.005$) yields a broadening $\Delta\nu_Q = 10(1)$ kHz of the satellite lines, which form the pedestal representing 85% of the total intensity. On the other hand, the impact of the quadrupole interaction on the width of the central line at 11.7 T, $\delta\nu_Q = (\Delta\nu_Q)^2/\nu_0 \approx 0.01$ kHz, is negligible compared to $\Delta\nu = 5.2$ kHz. It is worth noting that $\Delta\nu_Q$ and thus the EFG spatial dispersion $\langle(V_{zz} - \langle V_{zz}\rangle)^2\rangle$ do not vary with T.

Compared to $SrMnO_{3-\delta}$, $\Delta\nu_Q$ increases significantly in the La-doped samples, due to the charge disorder of the La^{3+}/Sr^{2+} cation sublattice. Nevertheless, the absence in the spectrum of any sign of a fine structure with satellite peaks [Figs. 3(b) and 3(c)] leads to a Sr charge environment characterized by $\langle V_{zz}\rangle = 0$. At room T and for the three samples, the equality $\langle V_{zz}\rangle = 0$ found by NMR agrees with the average cubic crystal symmetry deduced from the XRD results. At low T, as the equality $\langle V_{zz}\rangle = 0$ holds, we deduce that all three samples are also cubic in the AF phase.

2. *Magnetic broadening of the central line*

The magnetic broadening $\Delta\nu_M$ [28] is minimal in the PM phase of $SrMnO_{3-\delta}$, the central line of which has a Gaussian shape. For the La-containing oxides, the central line acquires an asymmetric shape due to spectral components with a larger value of the local magnetic field [Figs. 3(b) and 3(c)]. With decreasing T the width at half height of the central line, $\Delta\nu_M$, increases gradually, reaches a maximum at about 120 K (Fig. 4), and significantly diminishes down to 20 K.

In order to clarify the origin of the particular magnetic broadening that appears for the central line in the La-containing oxides, we first consider the shift of the ^{87}Sr NMR line (Fig. 5) in the PM state of $SrMnO_{3-\delta}$.

3. *Line shift and spin density of the doped electrons in* $SrMnO_{3-\delta}$

The Sr^{2+} ion has the configuration of inert Kr with filled valence electron shells plus an empty 5*s* shell. It is located at the center of the cubic unit cell so that the anisotropic dipolar and hyperfine fields created at the ^{87}I nucleus by the unpaired electrons of the eight first $Mn^{4+}(^3t_{2g}{}^0e_g)$ neighbors cancel each other. Thus, one should expect that the magnetic shift of the ^{87}Sr NMR line contains only the isotropic component, $^{87}K_{\text{iso}}$, which does not depend on the orientation of the crystallites in the magnetic field. As for ^{17}O NMR [23], the $^{87}K_{\text{iso}}$ value is

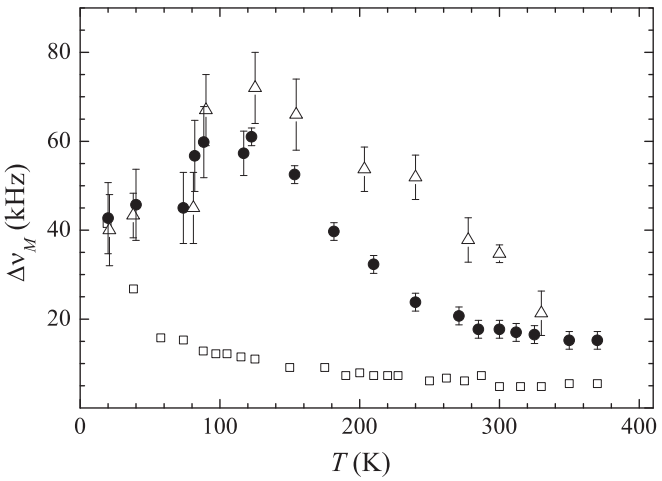

FIG. 4. Width of the central ^{87}Sr NMR line at 11.7 T, $\Delta\nu_M$, vs T in $x = 0.00$ (□), $x = 0.02$ (●), and $x = 0.04$ (△) samples.

determined by two contributions:

$$K(T,x) = K_0 + K_s(T,x). \tag{2}$$

The chemical shift $^{87}K_0$ is assumed to be independent of T and of the doped electrons concentration, where $x = 2\delta$ for $SrMnO_{3-\delta}$. The T-dependent shift $^{87}K_s(T,x) = {}^{87}K_{iso}(T,x) - {}^{87}K_0 = h_{loc}(5s)/H$ is related to the local field $h_{loc}(5s)$ appearing due to the Fermi contact interaction of the ^{87}I nuclear spin with the s-spin density of the itinerant doped electrons. The wave function of these doped electrons has mainly an e_g character [22,29,30] with a small admixture of the $5s$(Sr) and $2s2p$(O) states so that a spin density $s_z(5s) = f_s s_z(e_g)$ can be transferred from the e_g electron to the empty $5s$(Sr) orbital, f_s being the transferred fraction of $s_z(e_g)$. The e_g electron state is strongly polarized due to the intra-atomic exchange interaction, $-Js(e_g)S(t_{2g})$, with the core t_{2g}(Mn) electrons. As a result, the ensemble-averaged value of $s_z(5s)$ [31,32],

$$\langle s_z(5s)\rangle = f_s\langle s_z(e_g)\rangle = f_s g(E_F) J \langle S_z(t_{2g})\rangle, \tag{3}$$

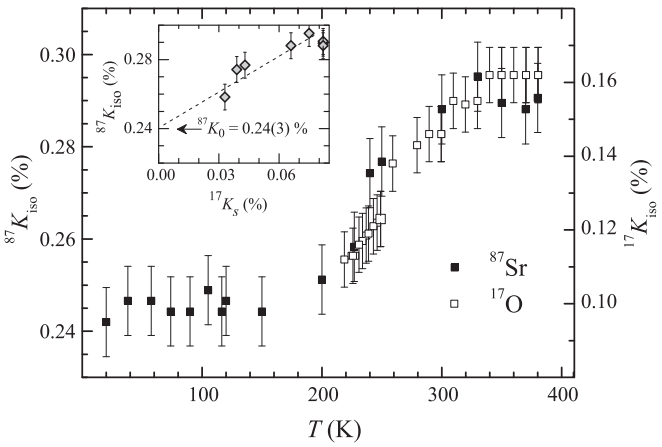

FIG. 5. Isotropic NMR line shifts $^{87}K_{iso}$ (■) and $^{17}K_{iso}$ (□) vs T in $SrMnO_{3-\delta}$. Inset: $^{87}K_{iso}$ vs $^{17}K_s$ plot, in the PM phase; the dotted line is a linear fit.

can be related to the local density of states of the doped e_g electrons, $g(E_F)$, and the spin susceptibility of the eight neighboring Mn atoms, $\langle S_z(t_{2g})\rangle = \chi_{mol}/2\mu_B N_A$. The expression for the spin contribution to the line shift, $^{87}K_s$, takes the form

$$\begin{aligned} {}^{87}K_s(T) &= h_{loc}(5s)/H = 8H_{FC}(5s) f_s \langle s_z(e_g)\rangle/H \\ &= 8H_{FC}(5s) f_s (J/E_F) n_{e_g} \langle S_z(t_{2g})\rangle/H, \end{aligned} \tag{4}$$

where $H_{FC}(5s)$ is the Fermi-contact field created by one unpaired electron occupying the $5s$(Sr) orbital, and n_{e_g} is the number of the itinerant doped electrons per Mn; n_{e_g} can vary with T but is always smaller than 2δ. A similar expression was obtained for $^{17}K_s$, the isotropic spin shift of the ^{17}O NMR line [23], containing the same T-dependent product $n_{e_g}\langle S_z(t_{2g})\rangle$ besides constant quantities. The similar thermal behavior of $^{87}K_{iso}$ and $^{17}K_{iso}$ shown in Fig. 5 confirms that expression (4) is valid for both nuclei. Furthermore, the significant decrease of both $^{87}K_{iso}(T)$ and $^{17}K_{iso}(T)$ below 300 K demonstrates that the local fields experienced by Sr nuclei and by O nuclei have the same microscopic origin, namely, the lessening of n_{e_g} with decreasing T.

As we are only interested in $^{87}K_s$, it should be extracted from $^{87}K_{iso}$. To that end, $^{87}K_{iso}$ is plotted vs $^{17}K_s$ in the PM phase (inset of Fig. 5). The linear fit of the data, extrapolated to $^{17}K_s = 0$, yields the chemical shift value, $^{87}K_0 = 0.24(3)\%$, which coincides with the total shift at 20 K, so that the doped electrons do not contribute anymore to $^{87}K_s$ at $T \leqslant 20$ K in $SrMnO_{3-\delta}$.

4. Inhomogeneous spin density of the doped electrons in the La-doped oxides

As in $SrMnO_{3-\delta}$, in the La-containing cubic oxides the ^{87}Sr magnetic shift reduces to the isotropic component so that the asymmetric shape of the lines [Figs. 6(b) and 6(c)] can only be explained with a shift distribution on the Sr atomic positions.

For $x = 0.02$ spectrum [Fig. 6(b)] the steepness of the low-frequency wing of the central line and its peak position are practically the same as for the central line in $SrMnO_{3-\delta}$ [Fig. 6(a)]. These similarities led us to decompose the spectra of the La-containing oxides in two lines [Figs. 6(b) and 6(c)]. For the symmetric line 1, the shift $^{87}K_{s1}$ and the width $\Delta\nu_M$ are taken equal to the corresponding parameters of $SrMnO_{3-\delta}$. Thus, the relative intensity of the line 1, Int_1, determines the fraction of the Sr atoms probing very few doped electrons ($2\delta < 0.01$), as in $SrMnO_{3-\delta}$. Its intensity decreases as the doping increases [inset in Fig. 6(a)], but is still nonzero for the most doped sample $x = 0.04$. For the other line, line 2, with an asymmetric shape, $g(K)$, we define its shift $^{87}K_{s2}$, as the gravity center, i.e., as the first moment of the line: $^{87}K_{s2} = \int (K - K_0) g(K) dK$; $^{87}K_{s2}$ is on the high-frequency side of the line 2 peak.

The inequality, $^{87}K_{s2} > {}^{87}K_{s1}$, shows that the Sr nuclei responsible for line 2 probe a larger number of e_g electrons compared to the Sr nuclei giving rise to line 1. A Sr ion contributing to line 2 defines an electron-doped region (EDR). The relative intensity of line 2, Int_2, determines the fraction of Sr atoms in the EDR containing presumably La^{3+} donors. At room temperature, Int_2 increases from 0.58(4) for $x = 0.02$ to

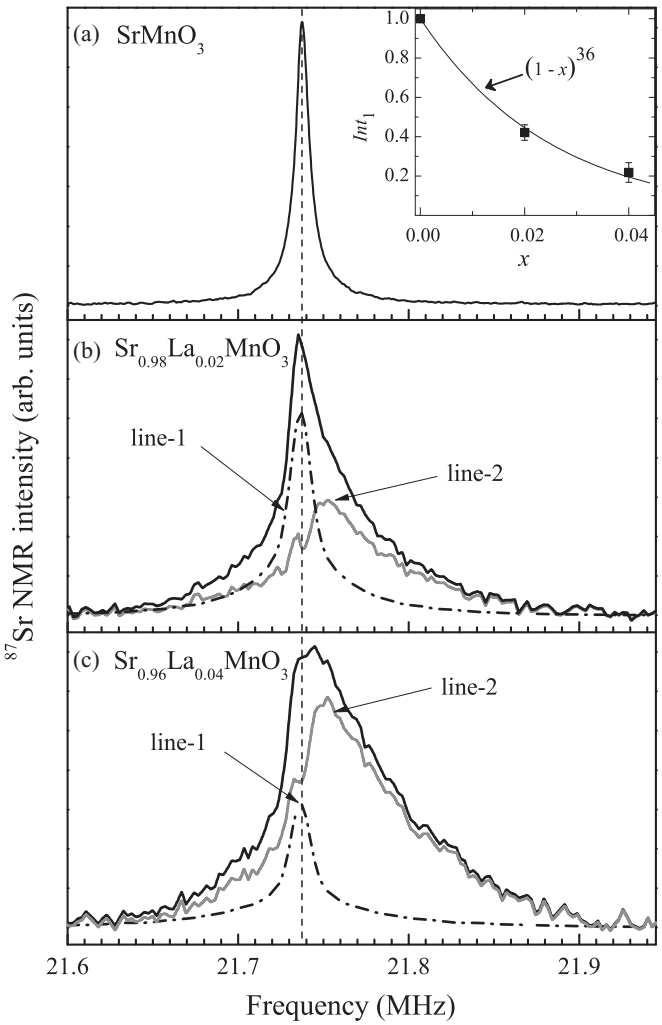

FIG. 6. ^{87}Sr NMR spectra, including all satellite transitions of $x = 0.00$ (a), 0.02 (b), 0.04 (c) samples at 11.7 T and room temperature. The dot-dashed (line 1) and gray (line 2) curves are the result of the spectrum decomposition in two lines as described in the text. Inset: relative intensity Int_1 of line 1 vs x and fit (dashed curve) with the binomial coefficient $P_{0,N} = (1 - x)^N$.

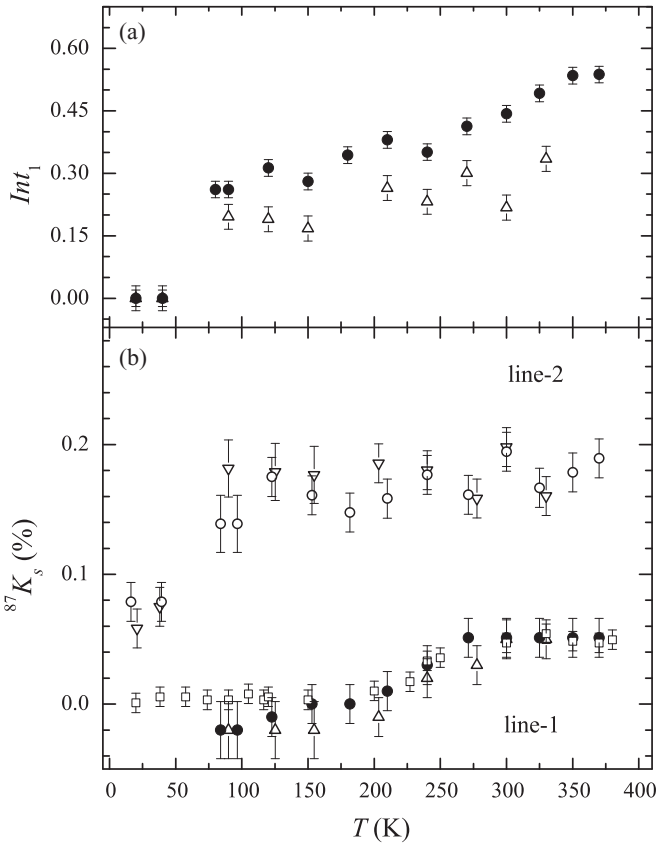

FIG. 7. (a) Relative intensity, Int_1, of line 1 vs T in $x = 0.02$ (•) and $x = 0.04$ (△) samples. (b) Shift, ^{87}K$_s$, vs T in $x = 0.00$ sample (□), in $x = 0.02$ for line 1 (•) and line 2 (○), in $x = 0.04$ for line 1 (△) and line 2 (▽) samples.

0.79(6) for $x = 0.04$. Assuming a random distribution of La^{3+} ions over the Sr^{2+} positions, one may estimate the average number of Sr^{2+} ions, N, which gather with some La^{3+} ions inside an EDR. The probability of this event is $1 - P_{0,N}$, where the binomial coefficient $P_{0,N} = (1 - x)^N$ defines the probability that no La is found among N randomly picked up cations (Sr/La). The $P_{0,N}$ value is directly connected to Int_1, and the corresponding fitting curve shown in the inset of Fig. 6(a) yields $N = 36 \pm 3$.

It is worth noting that for $x = 0.02$ and $N = 36$, the binomial probability $P_{1,36}$ that one La atom is in an EDR is significantly larger than $P_{2,36}$, the probability of two La atoms ($P_{1,36} > 3P_{2,36}$). A spherically shaped EDR with one La atom and $N = 36$ extends around the La atom to the distance $\approx 2a$. On the other hand, $N = 36$ overcomes $N_p = 31$ [33], the site percolation threshold in the 3D cubic lattice. Consequently, even for $x = 0.02$, the network of overlapping EDRs allows the motion of the doped electrons on large distances, explaining the metallic-like conductivity observed in single crystals of the same compounds at room temperature [8].

With decreasing T, the decrease of Int_1 [Fig. 7(a)] evidences a growth of Int_2 which is proportional to the EDR size, yielding an increasing overlap of the EDRs. Parallelly, $^{87}K_{s2}$ stays almost constant down to ~80 K [Fig. 7(b)]. In the AF-ordered phase, the FM moment per Mn of the in-field-canted AF G-type structure is $\langle m_{FM} \rangle = g\mu_B \langle S_z(t_{2g}) \rangle$. Its value is estimated from the slope of the $M(H)$ isotherms [Fig. 2(b)]. The $^{87}K_{s2}$ value is defined by the spatially averaged product $n_{e_g} \langle m_{FM} \rangle$, where n_{e_g} is the average density of the itinerant e_g electrons [23]. The growth of m_{FM} is negligible from 300 K to 150 K and significant down to 80 K; indeed, $[m_{FM}(150\text{ K}) - m_{FM}(300\text{ K})] < 0.05 m_{FM}(150\text{ K})$ whereas $[m_{FM}(80\text{ K}) - m_{FM}(150\text{ K})] \approx 0.25 m_{FM}(150\text{ K})$. As $^{87}K_{s2}$ is almost constant down to 80 K, n_{e_g} is almost constant down to about 150 K and then diminishes down to 80 K.

Simultaneously, the width of the shift distribution $\Delta K = \Delta\nu_M/\nu_0$ reaches a maximum at about 120 K (Fig. 4). As can be seen in Fig. 3(b), the growth of ΔK is caused by the Sr atoms with a large shift, $K_{s2,\text{large}}$, contributing to the NMR signal on the high-frequency side of line 2. A Sr atom with $K_{s2,\text{large}}$ is surrounded by eight neighboring Mn^{4+} ions the FM moment of which is aligned along H and larger than the spatial average value $\langle m_{FM} \rangle$. The $S(t_{2g})$ spins of these Mn^{4+} ions are

AF G-type ordered with an enhanced local canting due to the DE interaction with a number of itinerant electrons larger than the average value, n_{e_g}.

Below 100 K, only the data for the $x = 0.02$ sample will be analyzed since for $x = 0.04$ we showed that the sample is apparently a mixture of G- and C-type AF.

Below 50 K, as the line 1 disappears, $Int_1 = 0$ and the EDRs cover all the Sr positions [Fig. 7(a)]. Parallelly, the central line narrows, becoming almost symmetric [Figs. 3(b) and 3(c); $T = 20$ K] and $^{87}K_{s2}$ drops indicating that the Sr atoms having $K_{s2,\text{large}}$ do not contribute anymore to line 2. At low T the Sr sites with $K_{s2,\text{large}}$ are located inside the static FM entities and their ^{87}Sr NMR signal is shifted towards far larger frequencies [34], out of the NMR window corresponding to the Sr sites in the AF lattice (Fig. 3).

The residual value of $^{87}K_{s2} = 0.07(2)\%$ shows that about half of the e_g electrons are still itinerant so that two species of e_g electrons exist at $T < 50$ K. This NMR result is in agreement with electrical conductivity data performed on a single crystal of cubic $Sr_{1-x}La_xMnO_3$ with $x = 0.02$ which shows a metallic-like conductivity, $d\sigma/dT \leqslant 0$, with a residual conductivity $\sigma(T < 20\ \text{K}) \approx 2 \times 10^2\ \Omega^{-1}\ \text{cm}^{-1}$ [8]. This value is close to $\sigma_{\min} \sim 10^3\ \Omega^{-1}\ \text{cm}^{-1}$ the minimal metallic conductivity limit of Ioffe-Regel [35] near the Anderson transition. We will first focus on the itinerant electrons at $T < 50$ K.

C. Dynamics of the itinerant doped electrons in the AF phase of x = 0.02 compound

In the absence of structural and charge disorder, the itinerant e_g electrons [21,22,29] move fast with a characteristic intersite hopping time $\tau_{\text{hop}} = a/v_F = \hbar g(E_F) \approx 10^{-14}$ s. This value is significantly smaller than the period of the ^{87}Sr Larmor precession in 11.7 T, $2\pi/\gamma H \approx 5 \times 10^{-8}$ s. As a result, the Fermi gas of the itinerant e_g electrons creates a homogeneous ($q \approx 0$) spin polarization, $f_s\langle s_z(e_g)\rangle = f_s(2\mu_B)^{-1}\chi_s(q \approx 0)H$. In oxides, the resulting spin susceptibility, $\chi_s(q \approx 0)$, is generally not the Pauli susceptibility of the free electrons $\chi_P = 2\mu_B^2 g(E_F)$; it is rather $\chi_s(q \approx 0) = 2\mu_B^2 g(E_F)[1 - J(q \approx 0)g(E_F)]^{-1}$ enhanced by the factor $[1 - J(q \approx 0)g(E_F)]^{-1}$. In our case, the enhancement factor is due to the exchange interaction of the itinerant e_g electrons with the core t_{2g} electrons of the Mn^{4+} ions [31].

According to calculations of the electronic structure [22] in the AF G-type phase of an electron-doped cubic $SrMnO_3$, the Fermi level is located at the bottom of a rather broad conducting band, $W(e_g) \sim 0.5$ eV, where the density of electron states is almost constant with $g(E_F) \approx 1\ \text{eV}^{-1}\ \text{spin}^{-1}$. At small doping level, $x \ll 1$, this leads to a T-independence of $\chi_s(q \approx 0)$ and thus also of $^{87}K_s$ which is indeed observed for $^{87}K_{s2}$ in the $x = 0.02$ oxide at $T < 50$ K [Fig. 7(b)].

The dynamics of the itinerant doped electrons has been studied in the $x = 0.02$ sample by measuring the spin-lattice relaxation rate, $^{87}T_1^{-1}$, of the Sr nuclei. In the AF state, $^{87}T_1^{-1}$ decreases with a power-law dependence, $^{87}T_1^{-1} \propto T^{\alpha}$ where α is 3.5(5) above 120 K and changes to $\alpha = 1$ below 100 K, defining a linear behavior with $(^{87}T_1T)^{-1} = 0.020(6)\ \text{s}^{-1}\ \text{K}^{-1}$ (Fig. 8). It is worth noting that for magnetic semiconductors in the spin-wave region, below $T_N/2$, a typical T dependence

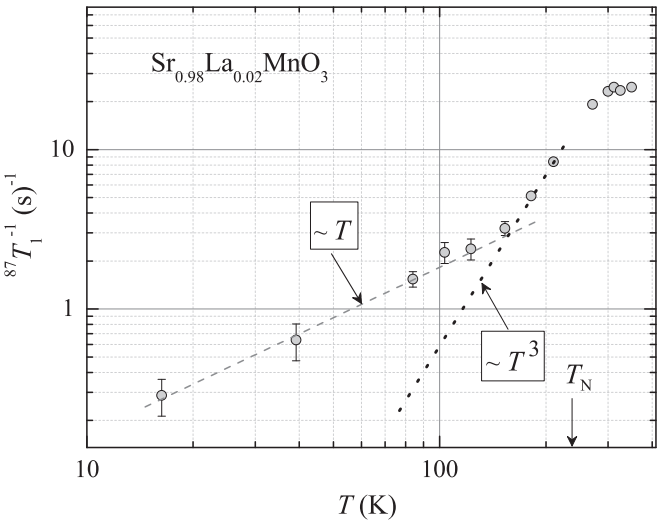

FIG. 8. Spin-lattice relaxation rate, $^{87}T_1^{-1}$, vs T in $Sr_{0.98}La_{0.02}MnO_3$.

is $T_1^{-1} \propto T^{\alpha}$ with $\alpha = 5$ due to fluctuations of the hyperfine interaction $\mathbf{IAS}$ which in our case would be $^{87}\mathbf{IAS}(t_{2g})$. Our $^{87}T_1$ data show that the $x = 0.02$ oxide is not in this case.

The Korringa law $(^{87}T_1)_K^{-1} \propto T$ is typical for nuclei of nonmagnetic ions in metals where the Fermi contact interaction with the conduction electrons provides an efficient mechanism at low temperature for the nuclear spin-lattice relaxation [36]. At small concentration n_{e_g} the interaction between the conduction electrons is negligible. As these electrons move in a crystal lattice with no random Coulomb potential, the $(^{87}T_1)_K^{-1}$ rate should be determined solely by the bare density of states at the Fermi level:

$$\left(^{87}T_1\right)_K^{-1} = 16\,^{87}\gamma^2 hk_B T[H_{FC}(5s)f_s g(E_F)]^2. \tag{5}$$

The Korringa product $^{87}C_K = {}^{87}(K_s^2T_1T)_K$ is a constant and does not depend on the electronic structure of the oxide:

$$^{87}C_K = {}^{87}\left(K_s^2T_1T\right)_K = \left(4\mu_B^2/{}^{87}\gamma^2 hk_B\right) = 2.76 \times 10^{-4}\ \text{s K}. \tag{6}$$

When the FM exchange interaction of the itinerant electrons with the core t_{2g} is taken into account the value of $^{87}K_s \propto \chi_s(q \approx 0)$ is enhanced by the factor $[1 - J(q \sim 0)g(E_F)]^{-1}$. Because of the high symmetry of the Sr site, the impact of this exchange interaction on the relaxation of the Sr nuclei has no peculiar q dependence so that $^{87}T_1^{-1}$ is still determined by the $(^{87}T_1)_K^{-1}$ term of Eq. (5) which relates to the $(q \approx 0)$ contribution to the nuclear spin-lattice relaxation. Thus, for e_g electrons interacting with t_{2g} electrons the corresponding Korringa product $^{87}C_K$ should be enhanced yielding

$$^{87}\left(K_s^2T_1T\right) = {}^{87}C_K[1 - J(q \approx 0)g(E_F)]^{-2}. \tag{7}$$

Although one expects that $^{87}(K_s^2T_1T) > {}^{87}C_K$, an opposite inequality is observed at $T < 50$ K where $^{87}(K_s^2T_1T)_{\text{exp}} = 0.32(6) \times 10^{-4}$ s K is one order of magnitude smaller than $^{87}C_K$. The discrepancy indicates that the $^{87}T_1^{-1}$ value is larger than in the Korringa prediction [Eq. (5)].

The imperfect shielding of the (La^{3+}/Sr^{2+}) charge disorder contributes to the scattering of the conduction electrons and consequently τ_{hop} increases yielding a weak localization [$\tau_{hop} > \hbar g(E_F)$] of the itinerant electrons in the metallic phase. Following Refs. [37,38], expression (5) is modified:

$$^{87}T_1^{-1} = \left(^{87}T_1^{-1}\right)_K \left[\tau_{hop}/\hbar g(E_F)\right], \quad (8)$$

where the enhancement factor $\eta = [\tau_{hop}/\hbar g(E_F)]$ takes into account a growth of τ_{hop}. On the metallic side of the metal-insulator transition the value of η is associated with the static conductivity by the following expression [38]:

$$\eta = {}^{87}T_1^{-1}/\left(^{87}T_1^{-1}\right)_K \approx 1 + (\pi/3)\left[\sigma_{min}^2/\sigma(\sigma + \sigma_{min})\right]. \quad (9)$$

The value $\eta = 8.6(8)$, obtained from the ratio $^{87}T_1^{-1}/(^{87}T_1^{-1})_K$, shows that the duration between two subsequent hops, τ_{hop}, is still larger than $\hbar g(E_F)$ corresponding to the de Gennes AF metallic phase [21]. It is worth underlining that the η value, deduced from NMR, leads to an estimate of the residual conductivity at low temperature, $\sigma \approx 1.3 \times 10^2\ \Omega^{-1}\ cm^{-1}$, close to $5 \times 10^2\ \Omega^{-1}\ cm^{-1}$, the conductivity measured in a single-crystal oxide with $x = 0.02$ composition [8].

D. Formation of magnetic polarons in the AF phase of x = 0.02 compound

The electrons which contribute no more to the line shift, $^{87}K_{s2}$, below 50 K have slowed down their motion. Their slow motion gives rise to low-frequency fluctuations of the Mn magnetic moments. Indeed, the electronic configuration of Mn ions changes during the time τ_c between two subsequent hops of an e_g electron, $^3t_{2g}{}^0e_g \rightarrow {}^3t_{2g}{}^1e_g \rightarrow {}^3t_{2g}{}^0e_g$, creating fluctuations of the Sr local field, $h_{loc}(5s)$, contributing to the spin echo decay rate, $^{87}T_2^{-1}$. In general [39] the main contribution to T_2^{-1} is caused by the fluctuating component $h_\parallel(t)$ directed along H, when $T_2^{-1} \gg T_1^{-1}$:

$$T_2^{-1} = \gamma^2 \langle h_\parallel(0)^2 \rangle \tau_c(T), \quad (10)$$

where $\langle h_\parallel(0)^2 \rangle$ is the square average of the fluctuating local field and $\tau_c \propto \exp(E_a/T)$ defines the thermal variation of the correlation function $\langle h_\parallel(t)h_\parallel(0)\rangle = \langle h_\parallel(0)^2\rangle \exp(-t/\tau_c)$. Our data show that below 150 K, the inequality $^{87}T_2^{-1} \gg {}^{87}T_1^{-1}$ holds.

When T decreases, τ_c becomes longer and the corresponding low-frequency fluctuations of $h_{loc}(5s)$ yield an increase of the spin echo decay rate, $^{87}T_2^{-1}$, of the Sr nuclei. This is seen in $Sr_{0.98}La_{0.02}MnO_3$ (Fig. 9) where $^{87}T_2^{-1}$ remains almost constant down to $T \sim 150$ K, and then increases up to a maximum at $T \approx 50$ K. Below 150 K a temperature-activated contribution to the spin echo decay rate, $(^{87}T_2^{-1})_a = [^{87}T_2^{-1}(T) - {}^{87}T_2^{-1}(150\ K)]$, increases following the Arrhenius law (Fig. 9, inset). The linear fit (dotted line) of the $(^{87}T_2^{-1})_a$ data above 50 K yields an estimate of the energy barrier $E_a = 460(100)$ K ≈ 40 meV which the e_g electron should overcome when hopping. At lower T, the electron is bound in a Coulombic potential and polarizes ferromagnetically the core spins of its surrounding. This interpretation is in agreement with the substantial growth of $M_{FM,sat}$ and N_{FM} below 50 K [inset of Fig. 2(b)].

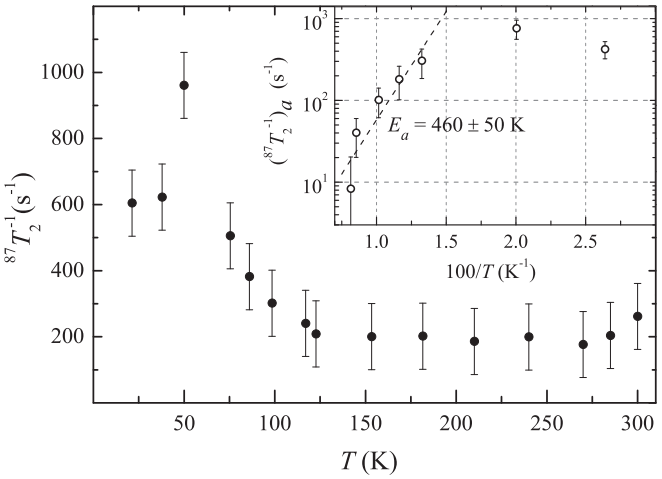

FIG. 9. ^{87}Sr echo-decay rate, $^{87}T_2^{-1}$, vs T in $Sr_{0.98}La_{0.02}MnO_3$. Inset: Arrhenius plot of $(^{87}T_2^{-1})_a = [^{87}T_2^{-1}(T) - {}^{87}T_2^{-1}(150\ )]$ vs $100/T$; the dashed line is a linear fit of the (T_2^{-1}) data above 50 K yielding the value of the energy barrier E_a.

It is reasonable to assume that the Coulombic potential appears around La^{3+} ions. According to ^{87}Sr NMR, magnetization, and ^{55}Mn NMR [24] data, these doped e_g electrons form static FM domains below 50 K. These FM entities can be considered as bound magnetic polarons (MPs) of small size with the effective moment $p_{eff} = 23(10)\ \mu_B$. A possible configuration of the MP is represented in Fig. 2(d).

The energy barrier, E_a, that the bound electrons must overcome to become itinerant is the energy of the MP formation. The E_a value obtained from $^{87}T_2$ measurements is, in fact, an ensemble average. Its distribution (±50 K; inset of Fig. 9) is due to the random distribution of the La atoms in the $x = 0.02$ compound. The Coulomb well depends also on the distribution of the La atoms in the compound. The deepest well appears probably around lone La^{3+} cations whereas for La atoms less distant from each other, the well is more extended and presumably less deep. In $Sr_{0.98}La_{0.02}MnO_3$ the energy of the MP formation is about 1.5 times larger than the value reported for cubic $SrMnO_{3-\delta}$ ($2\delta < 0.01$) oxides, where at low T, all 2δ electrons slow down [23,40] in the Coulomb wells of lone O^{2-} vacancies. Above about 50 K, the bound MPs are destroyed and only one species of doped electrons exists.

IV. CONCLUSIONS

The electron doped cubic $Sr_{1-x}La_xMnO_3$ perovskites were investigated by ^{87}Sr NMR. Three polycrystalline samples with different doping levels ($x = 0.00$, 0.02, 0.04) were studied in the paramagnetic (PM) and antiferromagnetic (AF) G-type phases ($T_N = 236$–200 K). The magnetic shift and magnetic broadening of the ^{87}Sr NMR spectra were analyzed. It is shown that the magnetic shift is proportional to the local density of the itinerant doped electrons surrounding the Sr sites; these electrons have mainly the e_g character. For the La-containing samples, the deconvolution of the inhomogeneously broadened spectra in two lines with distinct magnetic shifts and widths

allows clarifying the spatially distributed density of the itinerant doped electrons, which varies with the temperature and x. The intensity of the first NMR line determines the fraction of Sr atoms probing very few doped electrons whereas the Sr nuclei probing a larger number of e_g electrons give rise to a second line and define "electron-doped regions" (EDRs).

In the PM phase, all the doped electrons are itinerant. At room temperature the network of overlapping EDRs does not cover all Sr sites. Nevertheless, the estimation of the number of Sr sites inside an EDR exceeds the site percolation threshold in the 3D cubic lattice, even for $x = 0.02$, so that the electrons can move on large distances yielding a metallic-like dc conductivity.

The EDR overlapping enlarges with decreasing temperature. In the AF phase, below 80 K the EDRs cover the entire crystal. In this temperature range the doped electrons separate into two species. Indeed, a part of the electrons slow down their motion and form below 50 K static FM domains. These FM entities are considered as bound magnetic polarons (MPs) of small size with the effective moment $p_{\text{eff}} = 23(10)\ \mu_B$ and an MP formation energy of about 40 meV. The bound MPs are presumably located near lone La^{3+} ions. In $Sr_{0.98}La_{0.02}MnO_3$, the MP formation energy is about 1.5 times larger than in $SrMnO_{3-\delta}$ ($2\delta < 0.01$), where at low T, all 2δ electrons slow down. Above about 50 K, the bound electrons become itinerant, and the MPs are destroyed.

The second species concerns the doped electrons which remain itinerant at low temperature and participate in the fast hopping in the AF G-type ordered lattice of the Mn^{4+} ions. Nevertheless, their motion is slower than what is expected in an AF metal phase without cation disorder; this is probably due to the imperfect shielding of the (La^{3+}/Sr^{2+}) charge disorder.

At low temperature, contrary to the insulating state of $SrMnO_{3-\delta}$, in the metal phase of $Sr_{0.98}La_{0.02}MnO_3$, two species of doped electrons coexist. This electron separation is a consequence of the random distribution of the La atoms in heterovalent doped $SrMnO_3$ oxides.

ACKNOWLEDGMENTS

This work was performed as part of the state assignment of the Russian Federal Agency of Scientific Organizations (Program "Spin" No. 01201463330), supported in part by the Russian Foundation for Basic Research (Grant No. 16-02-00416), and by the Presidium of Ural Branch of Russian Academy of Sciences (Project No. 15-9-2-49). The authors thank B. Dabrowski and A. Yakubovskii for useful discussions. S.V. and A. Gerashenko are grateful to ESPCI Paris for hospitality and support.

[1] Y. Tokura, Rep. Prog. Phys. **69**, 797 (2006).
[2] C. Zener, Phys. Rev. **81**, 440 (1951).
[3] Y. N. Skryabin and Y. A. Izyumov, Phys. Usp. **44**, 109 (2001).
[4] M. Hennion, F. Moussa, G. Biotteau, J. Rodriguez-Carvajal, L. Pinsard, and A. Revcolevschi, Phys. Rev. B **61**, 9513 (2000).
[5] H. Terashita and J. J. Neumeier, Phys. Rev. B **71**, 134402 (2005).
[6] M. M. Savosta and P. Novák, Phys. Rev. Lett. **87**, 137204 (2001).
[7] O. Chmaissem, B. Dabrowski, S. Kolesnik, J. Mais, J. D. Jorgensen, and S. Short, Phys. Rev. B **67**, 094431 (2003).
[8] H. Sakai, S. Ishiwata, D. Okuyama, A. Nakao, H. Nakao, Y. Murakami, Y. Taguchi, and Y. Tokura, Phys. Rev. B **82**, 180409 (2010).
[9] J. J. Neumeier and J. L. Cohn, Phys. Rev. B **61**, 14319 (2000).
[10] E. Granado, C. D. Ling, J. J. Neumeier, J. W. Lynn, and D. N. Argyriou, Phys. Rev. B **68**, 134440 (2003).
[11] A. Maignan, C. Martin, F. Damay, B. Raveau, and J. Hejtmànek, Phys. Rev. B **58**, 2758 (1998).
[12] M. M. Savosta, P. Novák, M. Maryško, Z. Jirák, J. Hejtmánek, J. Englich, J. Kohout, C. Martin, and B. Raveau, Phys. Rev. B **62**, 9532 (2000).
[13] E. Dagotto, T. Hotta, and A. Moreo, Phys. Rep. **344**, 1 (2001).
[14] E. Nagaev, Phys. Rep. **346**, 387 (2001).
[15] J. M. D. Coey, M. Viret, and S. von Molnar, Adv. Phys. **48**, 167 (1999).
[16] K. R. Poeppelmeier, J. Solid State Chem. **59**, 71 (1988).
[17] E. O. Wollan and W. C. Koehler, Phys. Rev. **100**, 545 (1955).
[18] T. Negas and R. S. Roth, J. Solid State Chem. **1**, 409 (1970).
[19] O. Chmaissem, B. Dabrowski, S. Kolesnik, J. Mais, D. E. Brown, R. Kruk, P. Prior, B. Pyles, and J. D. Jorgensen, Phys. Rev. B **64**, 134412 (2001).
[20] J. L. Cohn, C. Chiorescu, and J. J. Neumeier, Phys. Rev. B **72**, 024422 (2005).
[21] P.-G. de Gennes, Phys. Rev. **118**, 141 (1960).
[22] A. M. Oleś and G. Khaliullin, Phys. Rev. B **84**, 214414 (2011).
[23] A. Trokiner, S. Verkhovskii, Z. Volkova, A. Gerashenko, K. Mikhalev, A. Germov, A. Yakubovskii, A. Korolev, B. Dabrowski, and A. Tyutyunnik, Phys. Rev. B **93**, 174413 (2016).
[24] A. Y. Germov, K. N. Mikhalev, S. V. Verkhovskii, Z. N. Volkova, A. P. Gerashchenko, A. V. Korolev, E. I. Konstantinova, I. A. Leonidov, and V. Kozhevnikov, JETP Lett. **102**, 727 (2015).
[25] S. Liu, X. Tan, K. Li, and R. Hughes, Ceram. Int. **28**, 327 (2002).
[26] Following Ref. [41] each $S(t_{2g})$ spin of the four Mn^{4+} ions [black balls in Fig. 2(d)] changes from $-3/2$ to $+3/2$ when flipped, contributing by 6 μ_B to $M_{\text{FM,sat}}$. In addition, 1 μ_B is due to the spin of the doped electron which aligns with the four $S(t_{2g})$ spins.
[27] A. Abragam, *The Principles of Nuclear Magnetism* (Clarendon Press, Oxford, 1961).
[28] The contribution of the dipole interaction to the width of the line is negligible compared with the experimental value $\Delta\nu_M$. Indeed, the homonuclear and heteronuclear contributions are only $(\Delta\nu)_{\text{Sr-Sr}} \approx 0.2$ kHz and $(\Delta\nu)_{\text{Sr-Mn}} \approx 1$ kHz, respectively.
[29] J. van den Brink and D. Khomskii, Phys. Rev. Lett. **82**, 1016 (1999).
[30] J. B. Goodenough, Phys. Rev. **100**, 564 (1955).
[31] A. Narath, *Hyperfine Interactions* (Academic Press, New York, 1967).
[32] E. A. Turov and M. P. Petrov, *Nuclear Magnetic Resonance in Ferro- and Antiferromagnets* (Halsted Press, New York, 1972).
[33] J. M. Ziman, *Models of Disorder* (Cambridge University Press, Cambridge, 1979).

[34] C. Kapusta and P. C. Riedi, J. Magn. Magn. Mater. **196-197**, 446 (1999).
[35] N. F. Mott, *Metal-Insulator Transitions* (Taylor & Francis, London, 1974).
[36] J. Korringa, Physica **16**, 601 (1950).
[37] W. W. Warren, Phys Rev. B **3**, 3708 (1971).
[38] Y. Zhdanov, A. M. Bogdanovich, B. A. Aleksashin, K. N. Mikhalev, V. V. Lavrentev, S. V. Verkhovskii, V. V. Serikov, and M. V. Sadovskii, Zh. Éksp. Teor. Fiz. **103**, 1762 (1993) [JETP **76**, 868 (1993)].
[39] C. P. Slichter, *Principles of Magnetic Resonance* (Springer-Verlag, Berlin, 1990).
[40] C. Chiorescu, J. L. Cohn, and J. J. Neumeier, Phys. Rev. B **76**, 020404(R) (2007).
[41] H. Meskine and S. Satpathy, J. Phys.: Condens. Matter **17**, 1889 (2005).